

# Lawrence Berkeley National Laboratory

## Recent Work

**Title**

ANGULAR DISTRIBUTIONS OF CHARGED PARTICLES FROM 31-Mev PROTONS ON CARBON

**Permalink**

<https://escholarship.org/uc/item/3488s5h1>

**Author**

Hecht, George J.

**Publication Date**

1955-04-21

UNIVERSITY OF  
CALIFORNIA

*Radiation  
Laboratory*

ANGULAR DISTRIBUTIONS OF CHARGED  
PARTICLES FROM 31-Mev PROTONS  
ON CARBON

TWO-WEEK LOAN COPY

*This is a Library Circulating Copy  
which may be borrowed for two weeks.  
For a personal retention copy, call  
Tech. Info. Division, Ext. 5545*

## **DISCLAIMER**

This document was prepared as an account of work sponsored by the United States Government. While this document is believed to contain correct information, neither the United States Government nor any agency thereof, nor the Regents of the University of California, nor any of their employees, makes any warranty, express or implied, or assumes any legal responsibility for the accuracy, completeness, or usefulness of any information, apparatus, product, or process disclosed, or represents that its use would not infringe privately owned rights. Reference herein to any specific commercial product, process, or service by its trade name, trademark, manufacturer, or otherwise, does not necessarily constitute or imply its endorsement, recommendation, or favoring by the United States Government or any agency thereof, or the Regents of the University of California. The views and opinions of authors expressed herein do not necessarily state or reflect those of the United States Government or any agency thereof or the Regents of the University of California.

UNIVERSITY OF CALIFORNIA

Radiation Laboratory  
Berkeley, California

Contract No. W-7405-eng-48

ANGULAR DISTRIBUTIONS OF CHARGED PARTICLES  
FROM 31-Mev PROTONS ON CARBON

George J. Hecht

(Thesis)

April 21, 1955

ANGULAR DISTRIBUTIONS OF CHARGED PARTICLES  
FROM 31-Mev PROTONS ON CARBON

Contents

Abstract . . . . .	3
Introduction	
A. Scattering Processes . . . . .	4
B. Angular Distributions . . . . .	6
1. Inelastic scattering . . . . .	6
2. Elastic scattering . . . . .	7
C. The Production of Deuterons . . . . .	8
Experimental Methods	
A. Beam Definition . . . . .	9
B. Scattering Chamber . . . . .	9
C. Targets . . . . .	11
D. Detectors and Electronics . . . . .	11
1. Scintillation counter and pulse-height analyser . . . . .	11
2. Differential range telescope and equipment . . . . .	12
E. Beam Monitor . . . . .	14
Reduction of Data	
A. Calibration of Pulse Height vs Energy . . . . .	15
B. Range-Energy Dependence . . . . .	15
C. Kinematics . . . . .	15
D. Differential Cross Section . . . . .	19
E. Errors . . . . .	20
Results and Conclusions	
A. Pulse-Height and Range Spectra . . . . .	22
B. Angular Distributions . . . . .	27
1. Elastic Scattering . . . . .	27
2. Inelastic Scattering . . . . .	29
3. Deuterons . . . . .	32
Acknowledgments . . . . .	35
References . . . . .	36

ANGULAR DISTRIBUTIONS OF CHARGED PARTICLES  
FROM 31-Mev PROTONS ON CARBON

George J. Hecht

Radiation Laboratory  
University of California  
Berkeley, California

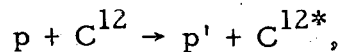
April 21, 1955

ABSTRACT

Angular distributions of several groups of charged particles resulting from the bombardment of carbon with 31-Mev protons have been obtained.

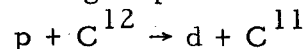
The angular distribution of elastically scattered protons is in good agreement with the prediction of the Born approximation at forward angles. Diffraction effects are compared with the results at lower energies and show that the angles for which they occur are not strictly proportional to  $\frac{\lambda}{R}$  over the energy range 10 to 31 Mev.

The angular distributions of two inelastic proton groups from the reaction



leaving  $C^{12*}$  with 4.43 Mev and 9.60 Mev excitation, have been analysed in accordance with the theory of Austern, Butler, and McManus. The theory apparently is inadequate for the 4.43-Mev level, in which both total angular momentum and parity for initial and final states are known. The shape of the angular distribution of the scattered protons corresponding to the 9.60-Mev level agrees with the theory and leads to an assignment of  $J' = 0^-, 1^-,$  or  $2^-$ .

A deuteron group from the reaction



has been identified and the angular distribution has been compared with the stripping theory of S. T. Butler by means of the principle of detailed balancing. The agreement found indicates that the ground state of  $C^{11}$  is characterized by  $J = 3/2^-$ .

ANGULAR DISTRIBUTIONS OF CHARGED PARTICLES  
FROM 31-Mev PROTONS ON CARBON

George J. Hecht

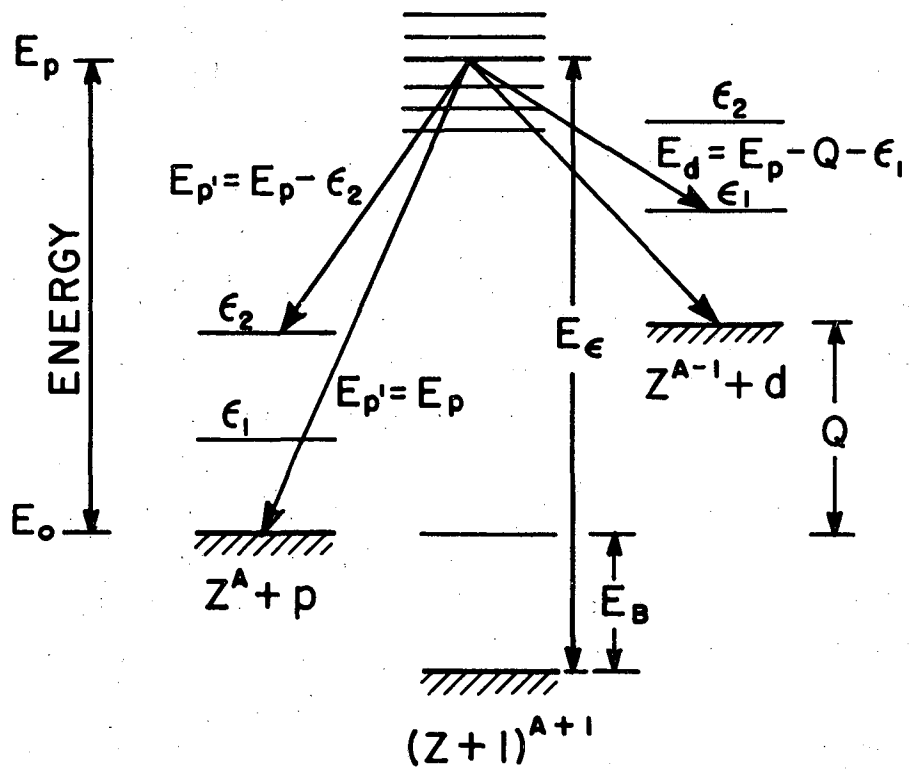
Radiation Laboratory  
University of California  
Berkeley, California

April 21, 1955

INTRODUCTION

A. Scattering Processes

The scattering of high-energy protons has been used since about 1940 to investigate the energy structure of nuclei and to provide at least qualitative concepts of the nature of nuclear forces. The experiments fall into two general classifications: resonance scattering and inelastic scattering. The energy relationships in the two processes are shown in Fig. 1. The original system  $Z^A + p$  consisting of target nucleus and incident proton has a rest energy  $E_0$ ; kinetic energy  $E_p$  of the system is plotted vertically above this reference and corresponds to the excitation  $E_\epsilon$  of the compound nucleus. If the compound nucleus emits a proton of energy  $E_p'$  less than  $E_p$  and goes to the system  $Z^A + p'$  (inelastic scattering), the difference in energy in the center-of-mass system between  $E_p'$  and  $E_p$  is the excitation of the target nucleus. Thus, observation of the energy spectrum of inelastically scattered protons reveals the excited levels of the target nucleus. If kinetic energy is conserved then the system returns to  $Z^A + p$ . Thus if  $E_p$  lies near a level of the nucleus  $(Z + 1)^{A + 1}$ , the cross section for the elastic process might show a peak as the incident energy  $E_p$  is varied through this region (resonance scattering). It is seen that in resonance scattering the binding energy  $E_B$  of the proton to the compound nucleus determines the lowest observable amount of excitation above the ground state of the nucleus  $(Z + 1)^{A + 1}$ , while in inelastic scattering all excitations of the target nucleus  $Z^A$  up to  $E_p$  are available.



MU-9305

Fig. 1. Energy-level diagram



## B. Angular Distributions

Early experiments, using either method, were concerned primarily with revealing the presence of excited levels and determining their energies and energy densities, whereas more recent experiments are concerned with the angular distributions of the scattered particles. The angular distribution yields information about the spins and parities of the levels involved.

### 1. Inelastic Scattering

In the inelastic scattering process, two general mechanisms are recognized. The first postulates the formation of the compound nucleus, which lasts long enough for the incident proton to share its energy with all the nucleons.<sup>1</sup> A proton will be emitted when the energy imparted to it by successive collisions becomes great enough for it to escape the nuclear well and penetrate the Coulomb barrier. The level density of excited states of the target nucleus increases with energy and atomic weight so that for heavy elements, the energy spectrum of emitted protons is continuous and exhibits the Maxwell-like distribution of a statistical system at a characteristic temperature.<sup>2</sup> Applying conservation of parity and total angular momentum as well as of z component of angular momentum yields the angular distribution of the scattered protons. Theory<sup>3, 4</sup> states that it is symmetrical about  $90^\circ$  in the center-of-mass system in cases where the level density is high enough to justify taking a statistical average and assuming that interference terms between outgoing waves of different parity cancel out.

The second mechanism assumes that the incident proton stays in the vicinity of the nucleus for a time of the order of its transit time across the nuclear diameter. The interaction is viewed as a nucleon-nucleon scattering event taking place in the peripheral region of the nucleus and resulting in an angular distribution that is peaked at forward scattering angles. This process is favored at higher incident energies where the absorption length<sup>5</sup> in nuclear matter is longer. Rhoderick<sup>6</sup> first observed such a nonsymmetric distribution for the inelastic scattering of 4.7-Mev protons from magnesium. Later experiments on carbon and magnesium<sup>7, 8, 9</sup> with protons of from 7 to 10 Mev and on beryllium and carbon at 31 Mev<sup>10</sup> confirm the character of the distribution.

Experiments on the heavy elements lead, gold, tantalum, and tin<sup>11</sup> at 31 Mev also revealed anisotropies in the angular distribution as well as showing that the energy distribution of the inelastic protons was almost flat rather than Maxwellian.

A theory for such peripheral scattering, proposed by Austern, Butler, and McManus,<sup>12</sup> relates the observed cross sections to the minimum allowable change in angular momentum of the proton (in  $\ell$  units of  $\hbar$ ). They give

$$\frac{d\sigma}{d\omega} \sim \left[ j_{\ell} \left( \left| \vec{k}_f - \vec{k}_i \right| a \right) \right]^2,$$

where  $k_i$  and  $k_f$  are the wave numbers in the center-of-mass system before and after scattering,  $a$  is the radius of the peripheral shell of the nucleus, and  $j_{\ell}$  is the regular spherical Bessel function of order  $\ell$ . Since this theory is based on the impulse approximation, a good fit with experiment can be expected only at small forward scattering angles. If the theory is valid, it provides a fairly powerful method of determining the total angular momentum and parity of excited levels when the corresponding quantities are known for the ground state. Finke<sup>13</sup> found fits with this theory for the excited levels of beryllium. In this case the probability of peripheral scattering is enhanced, since there is a very loosely bound nucleon circulating about a closed core of nucleons ( $\alpha$ -particle model).<sup>14</sup> The tightly bound structure of carbon, on the other hand, might be expected to suppress peripheral interactions and provide a more stringent test of the theory.

## 2. Elastic Scattering

The familiar Fraunhofer diffraction pattern of an opaque disk is a good approximation to the predictions of the optical model of the nucleus<sup>15, 5</sup> when applied to cases in which nuclear interaction far exceeds Coulomb scattering. For carbon, the ratio of total to Rutherford scattering approaches 30. The Born approximation applied to the wave functions representing incoming and outgoing protons produces essentially the same diffraction pattern. Consequently, the actual observed distribution would not be expected to agree with this theory at large scattering angles, where the Born approximation does not hold.

Cohen<sup>16</sup> has found many diffraction maxima and minima in elastic angular distributions at 22 Mev. From the optical analogue, one expects diffraction effects to be proportional to  $\frac{\lambda}{R}$  where  $\lambda$  is the wave length in the center of mass and R the nuclear radius. Cohen finds this  $1/R$  dependence to hold for elements from beryllium to thorium. In this experiment many carbon elastic data were taken with good accuracy.

### C. The Production of Deuterons

The production of deuterons from a target  $Z^A$  bombarded with protons may be regarded as the inverse reaction to the stripping of deuterons by a target  $Z^{A-1}$ . At 31 Mev Butler stripping theory<sup>17</sup> is appropriate, and the shape of the angular distribution of the cross sections for production is inferred from that for stripping if the principle of detailed balancing is invoked. In the inverse reaction, the shape of the angular distribution of the pickup deuterons provides a measure of the angular momentum change and parities. Daitch and French<sup>18</sup> demonstrate the equivalence of the Butler theory and the results of applying the Born approximation. They also show that if the interaction is considered to extend over the entire nuclear radius instead of taking place only in a peripheral region (the implicit assumption in the Butler theory) a modification in the shape of the angular distribution results which depends on the depth of the nuclear well for neutrons.

The energy Q (Fig. 1) is the minimum kinetic energy that must be given up in the center-of-mass system to produce deuterons. If energies higher than Q are lost the residual nucleus  $Z^{A-1}$  is left in an excited state.

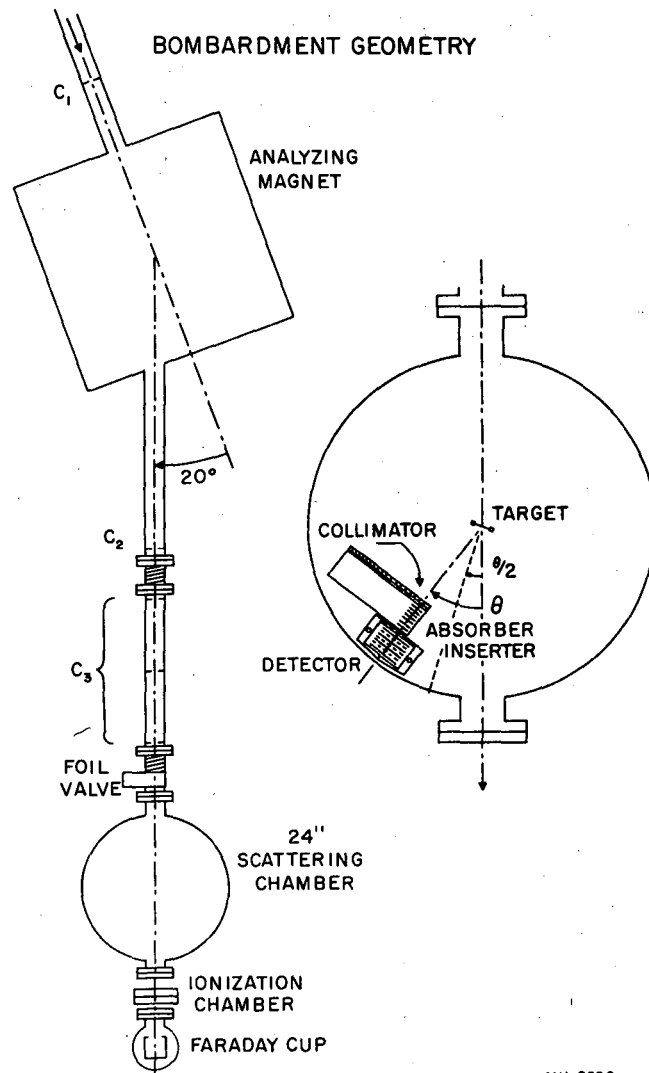
## EXPERIMENTAL METHODS

### A. Beam Definition

The beam from the linear accelerator has an angular divergence of  $10^{-3}$  radians, an energy spread of about 1 percent (full width at half maximum), and a diameter of 1/4 inch.<sup>19</sup> The beam is then further collimated by the system shown in Fig. 2. It consists of a remotely operated four-jaw premagnet collimator  $C_1$ , an analyzing magnet which deflects the beam through  $20^\circ$ , and an adjustable four-jaw postmagnet collimator  $C_2$  (set at aperture 1/8 inch by 1/8 inch), all primarily for restricting the energy spread. Beam shaping is accomplished by the collimator system  $C_3$ , consisting of a 1/8-inch circular aperture in a carbon disk followed at one-foot intervals by 5/32-inch and 3/16-inch apertures which limit slit scattering. The system  $C_3$  may be retracted for initial alignment without breaking the vacuum. The time-average beam current at the target is a maximum of  $3 \times 10^{-9}$  amperes with a maximum diameter of 3/16 inch. A picture of the beam, burned into a glass plate at the exit port of the scattering chamber, together with the postmagnet collimator, determines the beam line along which a telescope can be sighted to permit accurate alignment of the system  $C_3$  and the scattering chamber centerline.

### B. Scattering Chamber

The scattering chamber is 24 inches in diameter and contains a table which can be positioned in angle by remote control to within  $0.1^\circ$ . The lid of the chamber is provided with a remotely controlled target holder which can be positioned in angle to  $3^\circ$  and holds as many as six targets. If only one target angle is to be used for a run, it is possible to determine this angle to  $0.2^\circ$  by placing a front-surfaced mirror at one of the target positions and reading the table angle necessary to form an image of a reference point mounted on the table as seen through the telescope. Pressure inside the scattering chamber is maintained at less than  $10^{-5}$  mm of Hg by a local vacuum system.



MU-8590

Fig. 2. Bombardment geometry

### C. Targets

A 3-mil polystyrene (CH) foil was the primary target. However, the p-p scattering from the hydrogen in this target completely masks several of the levels of carbon at various forward scattering angles. Consequently, an almost pure carbon target was used at these angles. This target was prepared by gluing a thin block of carbon to the face plate of a lathe with Duco cement and then very carefully facing down the block to about 3 mils thickness. The cement was dissolved off with ether, and the target was carefully washed in alcohol and water and mounted in a metal frame. This process left some hydrogen (less than 1 percent), but no other impurities detectable in concentration to more than 1 percent. Targets prepared in this way from brittle substances like carbon are not entirely uniform in thickness over small areas, so that normalization to the CH elastic carbon cross section at  $60^\circ$  was made experimentally each time the target was used.

The targets were sufficiently thin so that less than 1 percent of the incident protons failed to be collected in the Faraday cup because of multiple Coulomb scattering. A useful approximate formula giving the multiple Coulomb scattering in thin targets to within 15 percent is

$$\overline{\theta^2} = \frac{dE}{E} \frac{Z}{1800},$$

where  $\overline{\theta^2}$  is the mean square scattering angle and dE is the energy loss of a proton of energy E in traversing a foil of atomic number Z.

### D. Detectors and Electronics

Two separate counting systems are employed: (1) pulse-height analysis of scintillation counter pulses, and (2) a differential-range proportional-counter method.

#### 1. Scintillation Counter and Pulse-Height Analyser

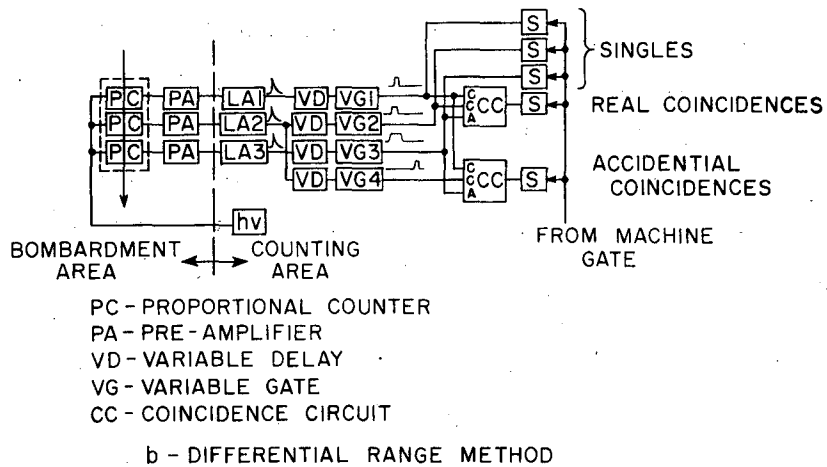
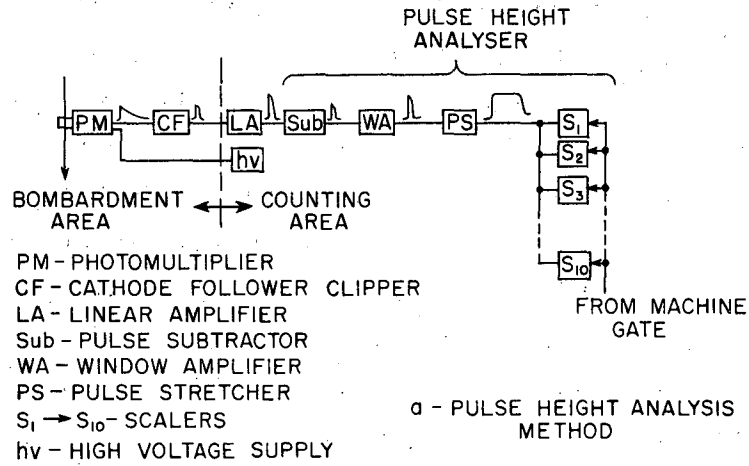
The scintillation counter consisted of a fast plastic scintillator (terphenyl in polystyrene) mounted on the face of a DuMont 6291 photomultiplier. The thickness of the scintillator is greater than the range of full-energy protons in this material. Output pulses are delay-line-clipped to about 1.0  $\mu$ sec in a cathode-follower clipping preamplifier, then fed into a linear amplifier the output of which drives the pulse-height

analyser, Fig. 3A. The analyser consists of a pulse subtractor, a window amplifier, and a pulse stretcher.<sup>20</sup> The output is then passed into ten 1024 scalers modified for differential pulse-height analysis with appropriate coincidence and anticoincidence circuits in each unit so that any particular count must fall in one and only one channel. Channel widths are adjustable from 0.1 to 10 volts. A great deal of effort was expended in stabilizing the analyser and removing long-term drifts. Over-all window stability is better than one percent for one- or two-volt windows. Since only ten scalers are available, a full pulse-height spectrum (0 to 100 volts) must be taken by sliding the windows along successive portions of the spectrum if reasonable window widths (1 to 2 volts) are used. The process of sliding the windows through many steps is not entirely reproducible and leads to uncertainties at low pulse heights. Enough scalers to record the entire spectrum simultaneously should eliminate this difficulty and decrease the required counting time as well.

Pulse-height resolution is as good as 3.5 percent (full width at half maximum) for 31-Mev protons stopping in the crystal. When the plastic scintillator is replaced by a pulsed light source of comparable light output a resolution of one to two percent is observed, indicating that the fundamental limitation in resolution is the variation of conversion efficiency (ionization energy into light). Total light collected for 31-Mev protons represents sufficient quanta to produce saturation in the output of the photomultiplier if operated at recommended voltages. Consequently reduced values of  $h\nu$  were employed; the actual value used was determined by maximizing the energy resolution and the linearity over the energy range 10 to 31 Mev. Better energy resolution could probably have been attained by using a sodium iodide crystal, but with the concomitant evils of surface impurity effects and higher background response to gamma radiation. The observed energy levels of carbon are sufficiently well spaced to obviate this need.

## 2. Differential Range Telescope and Equipment

In the differential range method, particles are detected in a telescope of three proportional counters of a type first used by Benveniste and Cork.<sup>21, 22</sup> A remotely controlled absorber changer is located



MU-9306

Fig. 3. Electronics block diagram



immediately in front of the telescope and behind an aperture which defines the solid angle for scattering. For a particular energy group of scattered particles, nearly enough absorber ( $R$ ) is introduced to stop the group. The degraded particles pass through two proportional counters, forming a coincidence, and stop in a  $\Delta R$  foil ( $\sim 6 \text{ mg/cm}^2$ ). A third proportional counter provides an anticoincidence pulse if a particle travels too far. So that no particles are lost because of multiple scattering in the counter foils, the counters have an aperture that subtends two root-mean-square scattering angles for the worst case of scattering encountered. Thus all particles with a range between  $R$  and  $R + \Delta R$  are counted. A plot of counts versus range yields the differential range curve of the group. Particles that stop in  $\Delta R$  produce pulses in the first two counters many times higher than the average noise pulse height, consequently a discriminator level may be set for pulse acceptance (plateau measurement). Discrimination level for the third counter is set just above the noise level in order to count all particles passing through  $\Delta R$ . Ashby<sup>23</sup> gives a complete analysis of this type of counter.

The three proportional counters are supplied by a common hv supply regulated to 0.1 percent. The preamplifiers (PA), linear amplifiers (LA), and variable gate (VG) units (Fig. 3B) are all of standard laboratory design. Gate widths from the first two counters are  $0.5 \mu\text{sec}$ , while the gate width from the third counter is  $1.5 \mu\text{sec}$  and overlaps both 1 and 2 in time. The worst jitter in electronics is in the response of Gate 3 with respect to Gates 1 and 2, and is  $0.5 \mu\text{sec}$ . The  $0.75\text{-}\mu\text{sec}$  overlap is sufficient cover for this jitter. Gate pulses are mixed in a diode coincidence circuit of time resolution of the order of  $0.1 \mu\text{sec}$ . Coincidences and singles are monitored with scalers (S). A fourth variable gate, fed by the delayed output of LA 2, is mixed with VG 1 and 3 in another coincidence circuit to monitor accidental coincidences.

#### E. Beam Monitor

A Faraday cup at the exit port of the scattering chamber collects the beam. The charge is integrated on a capacitor of value known to 0.1 percent. The potential across the capacitor is measured by a dc feedback electrometer and a recording millivoltmeter. Permanent

magnets at the entrance of the Faraday cup prevent escape of secondary electrons formed within the cup.

## REDUCTION OF DATA

### A. Calibration of Pulse Height vs Energy

A typical pulse-height distribution of the charged particles from carbon bombarded by 31-Mev protons appears in Fig. 4. The peaks (from right to left) correspond to the elastic peak, the 4.43-Mev level, the 9.6-Mev level, the 15-Mev level, and deuterons associated with the ground state of  $C^{11}$ . In particular, the energies for the first three peaks can be calculated precisely for any scattering angle, as the excitations involved are well known. Thus by varying the scattering angle one may generate a scintillator calibration curve of pulse height vs energy as in Fig. 5. It is seen that the dependence is linear to below 10 Mev. Some deuteron points are shown on this plot to illustrate that deuterons with  $dE/dx$  greater than that for protons at the same energy produce less light at the photocathode, a saturation effect of the scintillator. This type of energy calibration, although sufficient for the region of the first three peaks, is inadequate at lower energies for the precise determination of the energies of new levels, since the pulse-height analyser introduces uncertainties in regions of low pulse height (cf. Sec. D above).

### B. Range-energy Dependence

For a more precise energy determination of a particular group the range counter is used and a differential range spectrum is plotted. The energy is obtained from the range at the center of the peak by using Smith's range-energy plot.<sup>24</sup> For energies above 15 Mev the derived expression<sup>13</sup>

$$R = (\text{antilog } 0.4362) E_{\text{Mev}}^{1.778} + 2.0 \text{ mg/cm}^2$$

is employed.

### C. Kinematics

- (1) Transformation from laboratory to center-of-mass system  
For the reaction

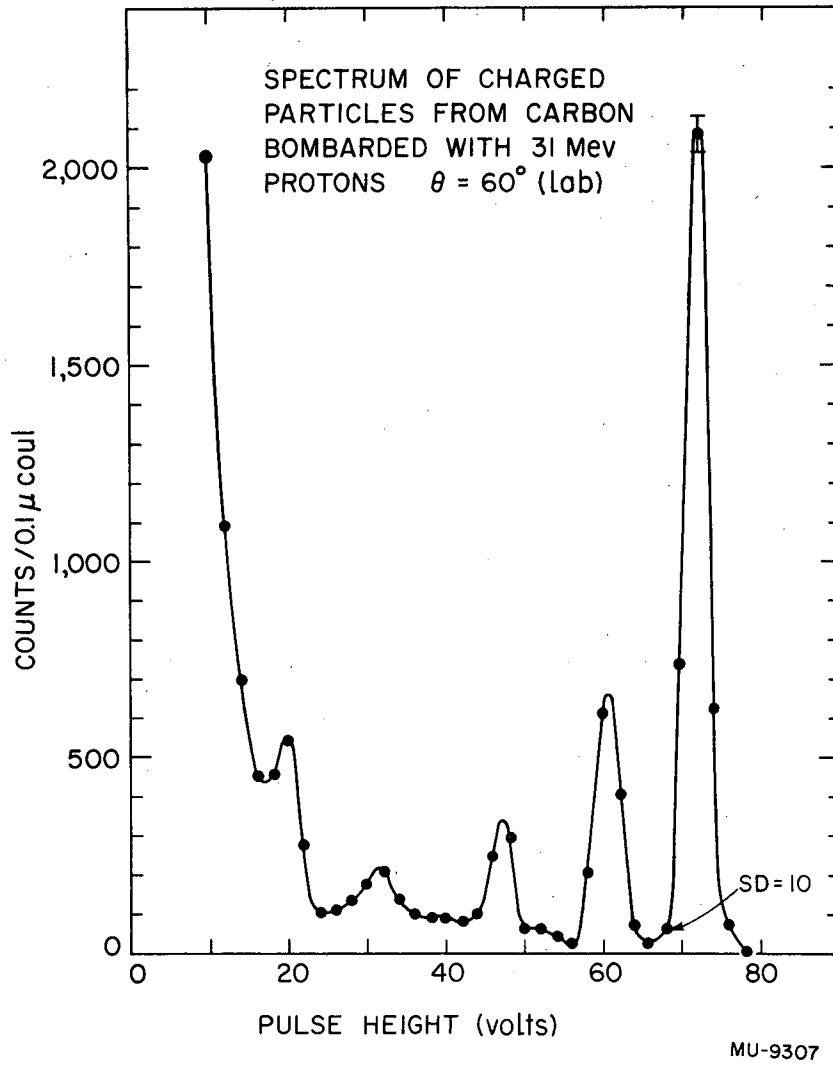


Fig. 4. Pulse-height spectrum

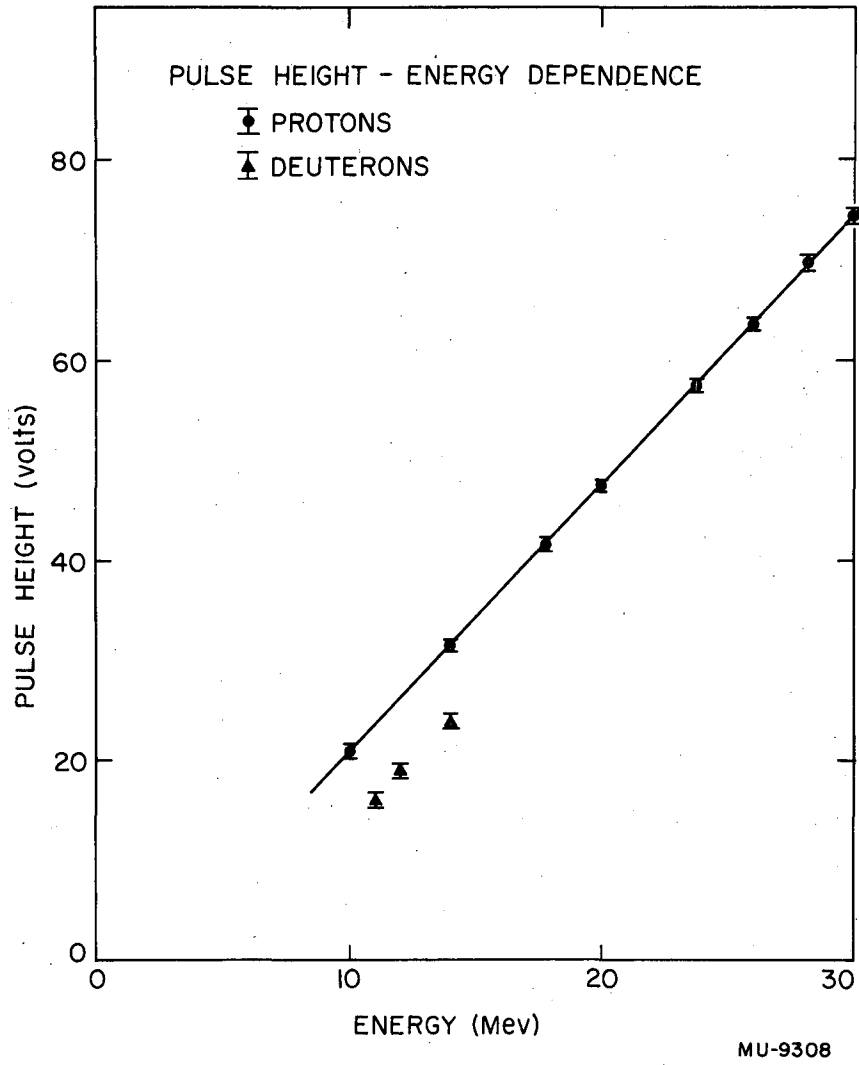


Fig. 5. Scintillator response

$$M_1 + M_2 + E_p \rightarrow M_3 + M_4 + \epsilon + E_f,$$

where  $\epsilon$  is the nuclear excitation energy,

$M_1$  and  $M_3$  are incident and outgoing particles,

$M_2$  and  $M_4$  are target and residual nuclei,

$E_p$  is the laboratory energy of the incident particle,

$E_f$  is the kinetic energy of the system after collision,

If  $\theta$  and  $\phi$  are the scattering angles (lab. and c.m.

respectively), and  $d\Omega$  and  $d\omega$  are the solid angle differentials (lab. and c.m. respectively),

the following nonrelativistic formulas apply:

$$\tan \theta = \frac{\sin \phi}{\cos \phi + r},$$

$$\cos \phi = \cos \theta \sqrt{1 - r^2 \sin^2 \theta} - r \sin^2 \theta,$$

$$\sin(\phi - \theta) = r \sin \theta,$$

$$\frac{d\omega}{d\Omega} = \frac{\sin \phi d\phi}{\sin \theta d\theta} = \frac{(r \cos \theta + \sqrt{1 - r^2 \sin^2 \theta})^2}{\sqrt{1 - r^2 \sin^2 \theta}},$$

and

$$\frac{1}{r^2} = \frac{M_2 M_4}{M_1 M_3} \left[ 1 + \left( \frac{M_1 + M_2}{M_2} \right) \frac{Q - \epsilon}{E_p} \right],$$

where

$$Q = [(M_1 + M_2) - (M_3 + M_4)] c^2.$$

(2) The lab. energy of particles scattered at angle  $\theta$  is

$$E_\theta = \frac{M_1 M_3}{(M_1 + M_2)^2} \frac{E_p}{r} \left[ r \cos \theta + \sqrt{1 - r^2 \sin^2 \theta} \right]^2.$$

For protons elastically scattered from  $C^{12}$  the incident energy

$E_p$  may be found from the scattered energy  $E_\theta$  and  $\phi$  by

$$E_p = 1.174 E_\theta \frac{\sin^2 \theta}{\sin^2 \phi}.$$

For deuterons leaving  $C^{11}$  in the ground state,  $E_p$  is found

from  $E_\theta$  and  $\phi$  by

$$E_p = 1.2803 \frac{\sin^2 \theta}{\sin^2 \phi} E_\theta + 17.86 \text{ Mev.}$$

(3) The excitation energy  $\epsilon$  of a level corresponding to a particular group of protons of energy  $E_\theta$  is

$$\epsilon = 0.9166 E_p - 1.083 E_\theta + 0.1666 \cos \theta \sqrt{E_p E_\theta}.$$

D. Differential Cross Section

In the center-of-mass system the differential cross section corresponding to a particle group scattering at an angle  $\theta$  is

$$\frac{d\sigma}{d\omega} = \frac{d\sigma}{d\Omega} \frac{d\Omega}{d\omega} = \frac{d\sigma}{d\Omega} f(\theta),$$

$$\frac{d\sigma}{d\omega} = N_s \frac{eM}{CV\Delta\Omega} \frac{\cos \theta_t}{t} f(\theta),$$

*thickness seen by particle*

where  $N_s$  is the total number of particles scattered into solid angle  $\Delta\Omega$ . Putting the quantities in conventional units and substituting for  $f(\theta)$  from the preceding section, we have

$$\frac{d\sigma}{d\omega} = N_s \left( \frac{eM \cos \theta_t \times 10^{36}}{C V t \Delta\Omega} \right) \left[ \frac{\sqrt{1 - r^2 \sin^2 \theta}}{r \cos \theta + \sqrt{1 - r^2 \sin^2 \theta}} \right]^2 \frac{\text{mb}}{\text{ster}},$$

where

- e is the charge of the electron in Coulombs,
- M is the mass of  $C^{12}$  in grams,
- C is the beam-integrating capacitance in  $\mu\text{farads}$ ,
- V is the electrometer potential in volts,
- t is the target thickness in  $\text{mg}/\text{cm}^2$ ,
- $\Delta\Omega$  is the solid angle of the counter at the target.

When data are taken with the pulse-height analyser,  $N_s$  is simply  $\sum_i (N_i - B_i)$ , where  $N_i$  and  $B_i$  are the number of total counts and background counts in the  $i$ th channel, respectively. ( $B_i$  is approximated by drawing smooth curves through the minima of the pulse-height spectra.)

For the differential range method,

$$N_s = \frac{1}{\Delta R} (A - B) = \frac{1}{\Delta R} \left[ \int \left( \frac{dN}{dR} \Delta R \right) dR - B \right],$$

where A is the area under a peak (gaussian) of the differential range curve and B is the total background (again estimated by drawing smooth curves through the minima of the spectrum).  $\left( \frac{dN}{dR} \Delta R \right)$  is the quantity actually measured at each range point R. The area A is found by fitting a triangle through the experimental points. The area of a triangle whose sides are tangent to a gaussian at the points of inflection, is 0.968 the area of the gaussian.

E. Errors

In terms of measured quantities the cross section is given by

$$\frac{d\sigma}{d\omega} = N_s \frac{\cos \theta_t}{CV \Delta \Omega t} f(\theta).$$

For a functional dependence of the form

$$y = \prod_j x_j^{a_j},$$

the law of propagation of errors gives

$$\frac{\delta y}{y} = \left[ \sum_j \left( a_j \frac{\delta x_j}{x_j} \right)^2 \right]^{1/2}$$

Listing the terms separately, we find

$$\frac{\delta c}{c} = 0.1\%,$$

$$\frac{\delta V}{V} = 0.5\%,$$

$$\frac{\delta(\cos \theta_t)}{\cos \theta_t} = \tan \theta_t \delta \theta_t \quad \theta_t = 45^\circ \quad \delta \theta = 0.2^\circ = 0.0035 \text{ radian,}$$

$$\frac{\delta(\cos \theta_t)}{\cos \theta_t} = 0.35\%,$$

$$\frac{\delta(\Delta \Omega)}{\Delta \Omega} = 2.6\%,$$

$$\frac{\delta t}{t} = 0.1\% \text{ for CH targets and } 5\% \text{ for carbon targets,}$$

$$\frac{\delta f(\theta)}{f(\theta)} = 0.1\% \text{ for } \delta \theta = 0.1^\circ.$$

If the cross section for a reaction is a rapidly varying function of angle, then the uncertainty of  $0.1^\circ$  in table setting may contribute as much as 0.8 percent uncertainty in cross section (elastic scattering at  $20^\circ$ ). All the above errors combine to give a relative error of 5.7 percent. To this figure must be added the contribution to the error from  $N_s$ . For the scintillation counter method

$$\frac{\delta N_s}{N_s} \text{ is estimated by } \sqrt{\frac{\sum_i (N_i + B_i)}{\sum_i (N_i - B_i)}} \text{ . (counting statistics)}$$

For the differential range method

$$\left\{ \frac{\delta N_s}{N_s} \right\} = \left[ \left( \frac{\delta(\Delta R)}{\Delta R} \right)^2 + \left( \frac{\delta(A-B)}{A-B} \right)^2 \right]^{1/2}$$

Here  $\frac{\delta(\Delta R)}{\Delta R} = 0.9\%$ , and  $\frac{\delta(A-B)}{A-B}$  depends on the counting statistics

but is estimated directly from the data by determining the range in value of (A - B) for possible triangles making good fits with the data.

Many independent observations impart confidence in the method. In the best cases (elastic data),  $\frac{\delta(A-B)}{A-B}$  is 3 percent while an average

value might be 7 percent. The total combined relative error becomes

6.0% for 2% statistics (best data)	}	for the scintillation method,
7.6% for 5% statistics (average)		
6.5% for 3% error in A (best data)	}	for the differential range method.
9.6% for 7% error in A (average)		

It is seen that the total relative error in cross section for the two methods is quite comparable for the best data taken. The calculated error, however, takes no account of contributions to the error in  $N_s$  due to background variations or to shifts in beam energy during runs. The former can be detected when background shifts of more than 10 percent occur and is a source of trouble common to both methods. The latter contributes no error to the cross section as determined by analysis of the pulse-height data, since all channels bracketing a peak record simultaneously, and thus no counts are lost or counted twice. Shifts in beam energy may introduce as much as 20 percent uncertainty in cross section for data taken with the differential range method for processes with low cross section. Fundamentally then the scintillation counter can produce more accurate cross sections than the differential range method and requires much less running time. At low energies, however, background due to neutron and gamma radiation from the linear accelerator becomes a serious problem in analysing the pulse height data, since the target-in—target-out method requires the finding of a relatively small difference between two relatively large numbers. There is a physical limit to the amount of shielding that can be introduced to reduce this background. A thin proportional counter or very thin scintillator in front of the analysing crystal to produce a coincidence for heavy charged particles only would be an improvement.



The differential range counter with its coincidence requirement is free from this limitation, and exhibits practically no target-out background. Its superior energy resolution ( $\sim 1.8\%$ ) permits estimation of energies of peaks to about 0.1% (0.03 Mev at 30 Mev).

An additional practical consideration in the operation of the scintillation counter is that the maximum counting rate is determined by the counting rate of all particles stopping in the crystal, not just the group being analysed, in contrast to the proportional counter telescope, where most of the particles passing entirely through the telescope have too low a  $dE/dx$  to contribute to pile-up.

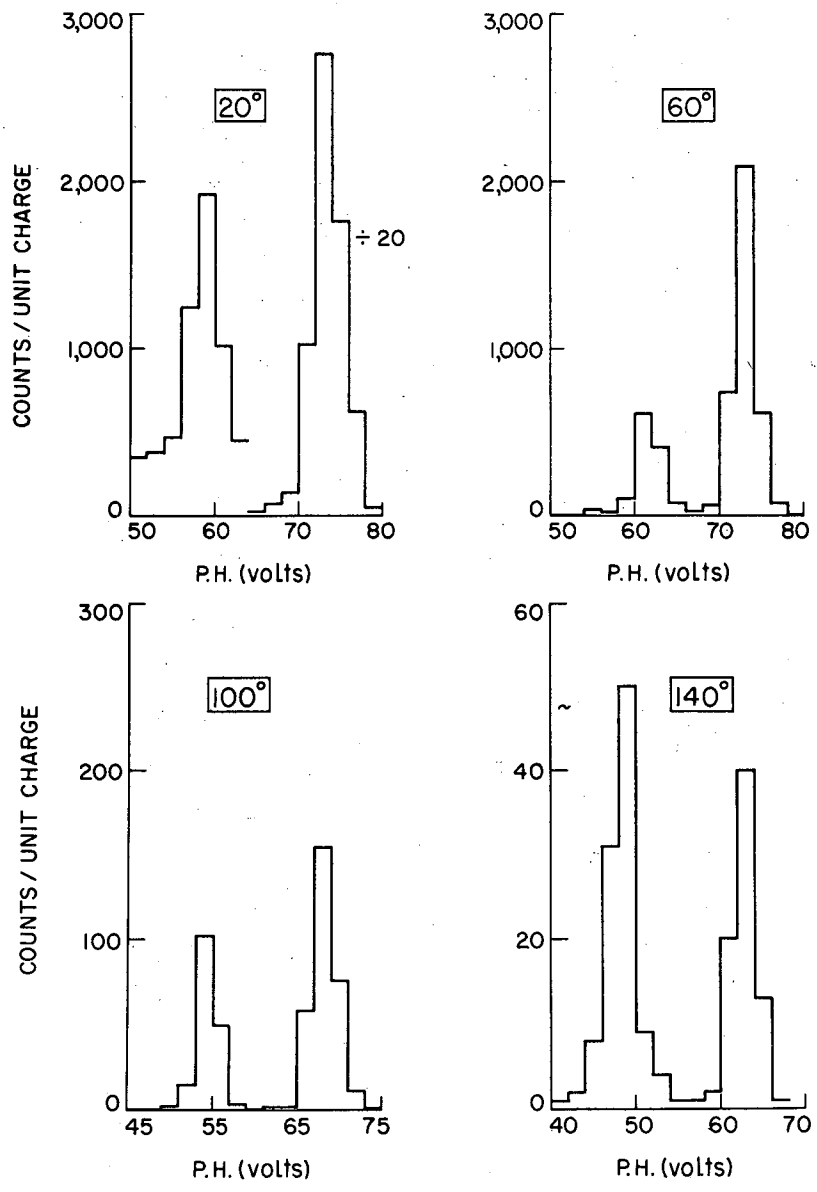
In the light of these considerations it is seen that the most advantageous way to employ the two methods is to restrict the use of the scintillation counter to that portion of the high-energy region of the spectrum for which target-out background is negligible.

## RESULTS AND CONCLUSIONS

### A. Pulse-Height and Range Spectra

Pulse-height distributions similar to those shown in Fig. 4 were taken at  $30^\circ$ ,  $40^\circ$ ,  $50^\circ$ ,  $60^\circ$ ,  $80^\circ$ ,  $100^\circ$ ,  $120^\circ$ , and  $140^\circ$ . In all spectra the elastic peak and the peaks corresponding to the 4.43-Mev and 9.6-Mev levels appear prominently. The peak corresponding to the 15-Mev level is too small to be identified at angles less than  $45^\circ$  and is masked by background at angles greater than  $80^\circ$ . A level of 7.6-Mev excitation is known to exist<sup>14</sup> and considerable effort was expended in attempting to detect it in this experiment, but within reasonable running times it could not be found above statistical uncertainty at any angle.

As noted previously, the pulse-height analyser is most reliable if restricted to the higher pulse-height regions. Consequently the angular distribution of the elastic group and the group corresponding to the first excited level were taken from the pulse-height data. Spectra similar to those shown in Fig. 6 were taken at  $5^\circ$  intervals at all angles from  $10^\circ$  to  $170^\circ$  in the laboratory system and with a statistical accuracy of at least 2 percent for the elastic group and an average of 5 percent for the 4.43-Mev level.



MU-9309

Fig. 6. Pulse-height distributions of protons corresponding to ground state and first excited level of  $C^{12}$

Complete differential range spectra were taken at  $15^\circ$ ,  $30^\circ$ ,  $45^\circ$ ,  $60^\circ$ ,  $90^\circ$ , and  $120^\circ$ , some of which are shown in Fig. 7. Although these spectra are much more tedious to take (since only one range point is obtained at a time), this method eliminated the possibility of finer structure in the peaks of the pulse-height spectra. In addition, independent confirmation of the cross sections obtained from pulse-height data was provided. In the differential range spectrum of  $60^\circ$  the peaks are (from right to left) the elastic group, the 4.43-Mev level, the 9.6-Mev level, the 15-Mev level, and a small group of deuterons just to the right of the large peak of protons. The protons in this large peak are those scattered by hydrogen in the CH target that was used for this particular run. These two groups (deuterons and protons) would not have been resolved by the scintillator at this angle. In the differential range spectrum at  $30^\circ$ , there is a small peak between the proton groups corresponding to the 4.43-Mev and 9.60-Mev levels. This peak is due to the hydrogen impurity left in a "carbon" target and corresponds to less than one percent of the peak that would be present from a CH target. The width of the peak is greater than the width of the proton groups on either side because the energy of protons scattered from hydrogen is a steep function of scattering angle, and for the fixed angular aperture of the counters ( $\sim 1.6^\circ$ ) a rather large energy dispersion results.

In addition to the complete spectra listed, all data presented for the 9.6-Mev level as well as those for the pickup deuterons were obtained with the differential range method. The deuteron group observed is from the reaction  $p + C^{12} \rightarrow d + C^{11}$  leaving  $C^{11}$  in the ground state ( $Q = -16.49$  Mev). Positive identification of the deuterons was made possible by taking advantage of the fact that the first two counters can be used to measure the  $dE/dx$  of particles that stop in  $\Delta R$ . Since the  $dE/dx$  of deuterons, of the same residual range as protons, exceeds the  $dE/dx$  of protons by about 30 percent, a similar difference in pulse height in the first two counters should be observable. Figure 8 shows the result of plotting counting rate against discrimination level of the first two counters for elastic protons ( $R = 1200 \text{ mg/cm}^2$ ) and the suspected deuterons ( $R = 165 \text{ mg/cm}^2$ ) from the data taken at  $30^\circ$ . The plateau is definite in both cases and is seen to be about 35 percent longer for the second group, hence these particles are certainly deuterons.

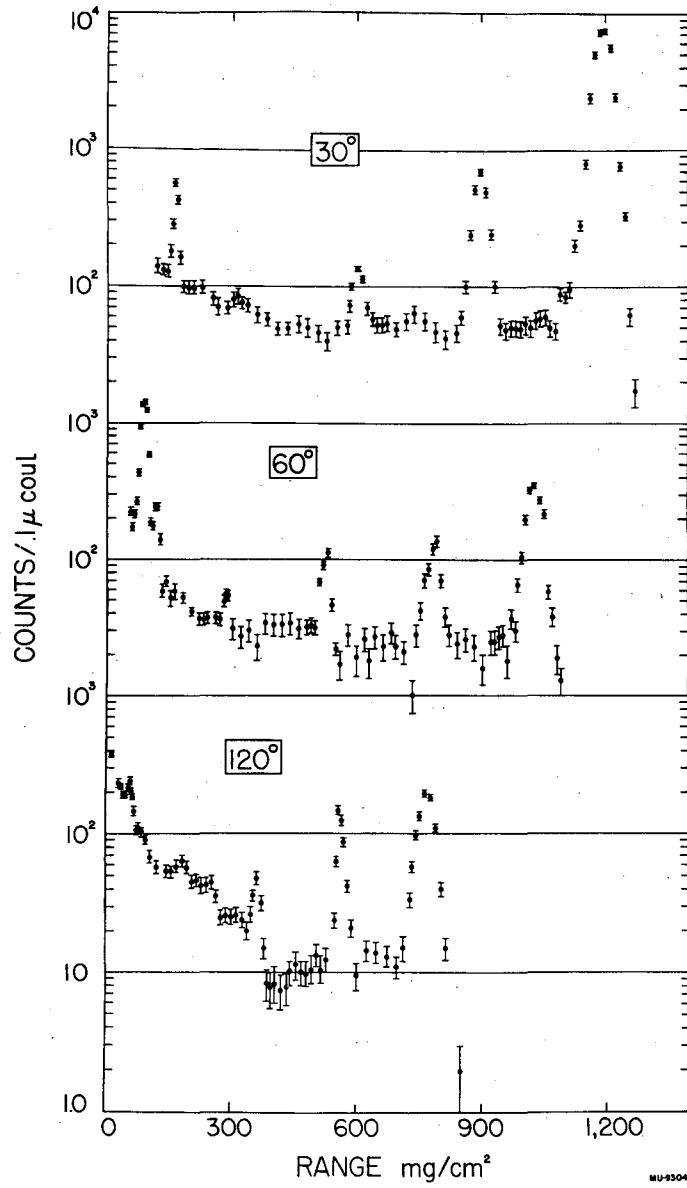
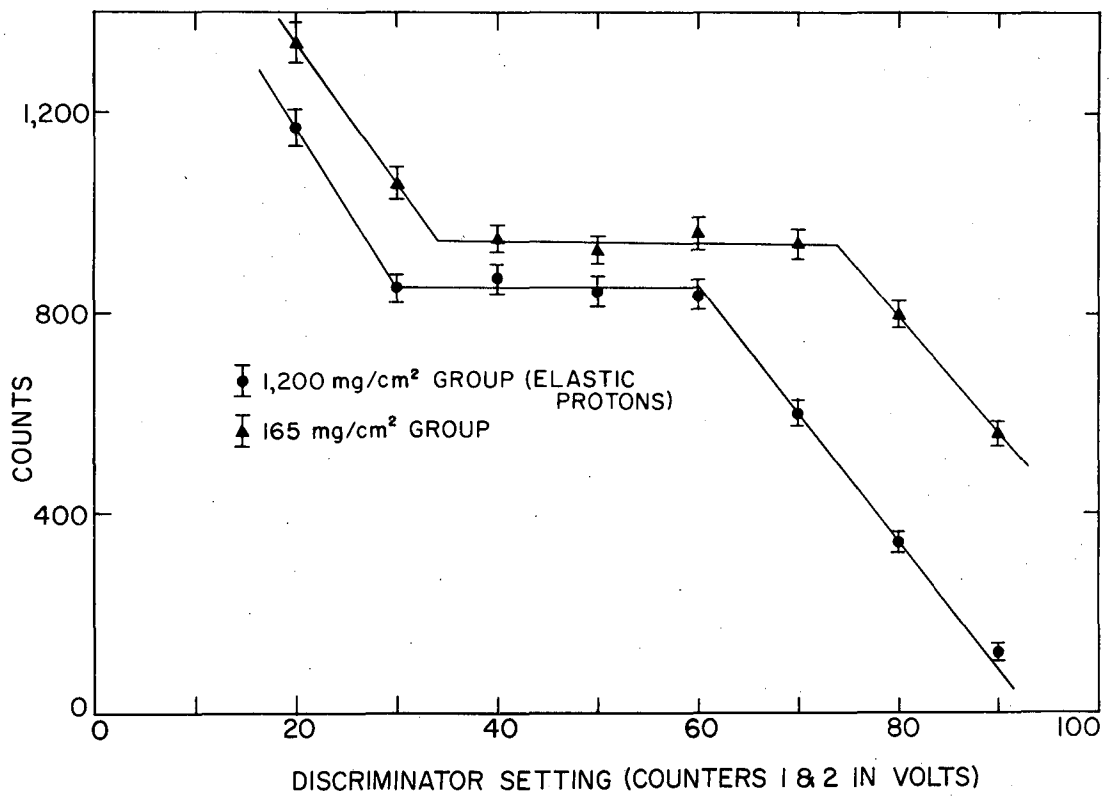


Fig. 7. Differential range spectra



MU-9313

Fig. 8. Particle identification by  $dE/dx$  measurement

The excitation energies of the observed levels as measured from analysis of the differential range spectra are

$$\begin{aligned} &4.43 \text{ Mev} \pm 0.05 \text{ Mev,} \\ &9.60 \text{ Mev} \pm 0.08 \text{ Mev,} \\ &14.98 \text{ Mev} \pm 0.11 \text{ Mev.} \end{aligned}$$

In addition to these levels, there is evidence suggesting the existence of a level of low cross section of 21.9-Mev excitation as well as the existence of several very broad levels or many sharp ones of excitation between 11 and 20 Mev which appear in the spectra taken at backward angles. Many levels are known to exist in this region from experiments with deuterons and alphas as the bombarding particles.<sup>14</sup>

## B. Angular Distributions

### 1. Elastic Scattering

The differential cross section for elastic scattering has been measured at 33 angles with the scintillation counter and confirmed at 6 angles with the differential range method. The angular distribution is plotted in Fig.9 and compared with the results of the Born approximation, which gives an angular dependence

$$\frac{d\sigma}{d\omega} = \left[ \frac{j_1(2ka \sin \phi/2)}{2ka \sin \phi/2} \right]^2$$

The value for the nuclear radius producing a best fit to the experimental angular distribution at forward angles is  $a = 1.80 \times A^{1/3} \times 10^{-13}$  cm. Clearly the behavior at large angles does not fit this simple theory. The rather large value of the nuclear radius required to fit the data at forward angles seems characteristic of this type of matching (in the case of Be<sup>9</sup>, a radius of  $1.90 \times A^{1/3} \times 10^{-13}$  cm was required<sup>13</sup>), and is not considered a significant measure of true nuclear size.

The ratio of the observed differential scattering cross section to the cross section calculated for pure Rutherford scattering yields maxima and minima at angles that can be compared to the results at 10 and 22 Mev.<sup>9, 16</sup> If  $\phi \propto \lambda/R$  and if R is independent of energy then

$$\frac{\phi_{E_1}}{\phi_{E_2}} = \frac{\chi_{E_1}}{\chi_{E_2}} = \sqrt{\frac{E_2}{E_1}},$$

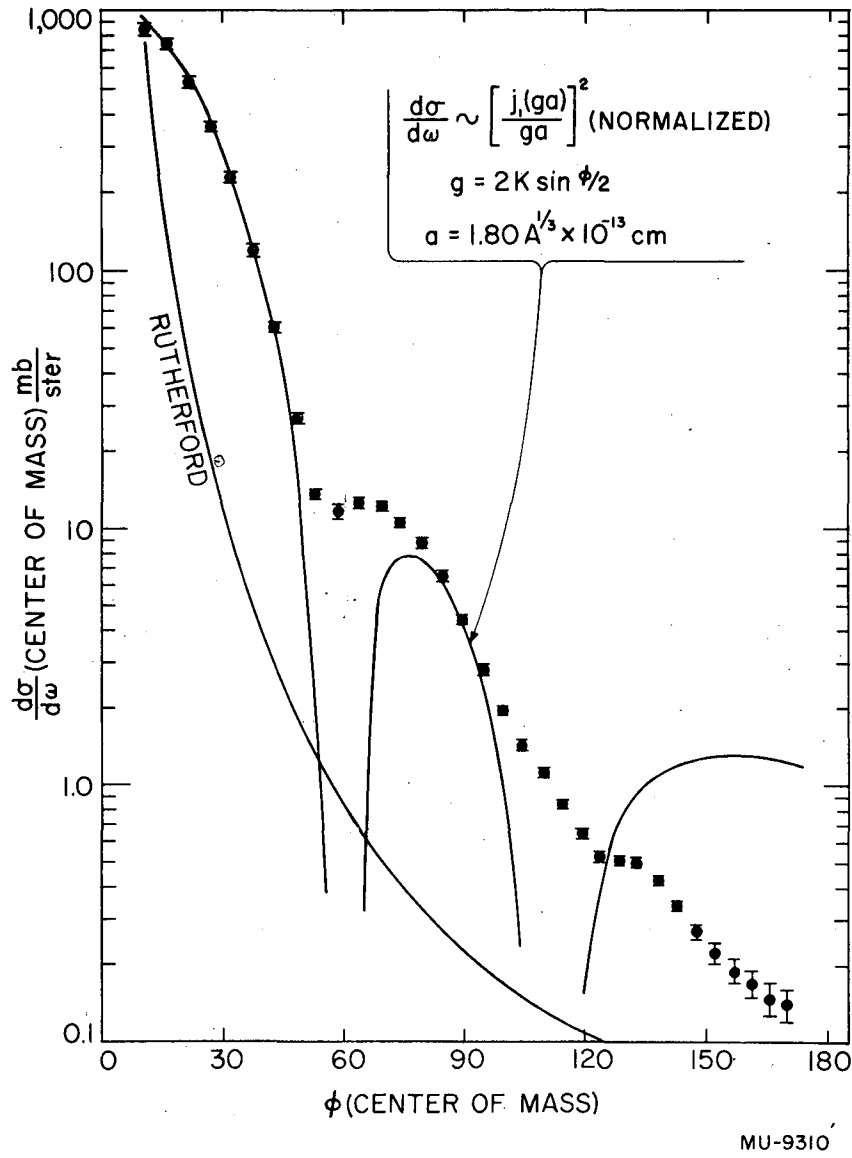


Fig. 9. Angular distribution of the differential cross section for elastic scattering of protons from  $C^{12}$  at 31 Mev (lab) and the Born approximation prediction

so that the angles at which the effects occur, at different energies, should be related by the factors

$$\frac{\phi_{10}}{\phi_{22}} = 1.48, \quad \frac{\phi_{22}}{\phi_{31}} = 1.19, \quad \frac{\phi_{10}}{\phi_{31}} = 1.76 .$$

The factors actually found are listed below.

	Angles at which effects occur			$\frac{\phi_{10}}{\phi_{22}}$	$\frac{\phi_{22}}{\phi_{31}}$	$\frac{\phi_{10}}{\phi_{31}}$
	10 Mev	22 Mev	31 Mev			
max.	50	36	34	1.39	1.06	1.47
min.	--	55	53	--	1.04	--
max.	120	88	80	1.37	1.10	1.50

The results produce factors smaller than those predicted and might indicate that the nuclear radius cannot be considered to be independent of energy over this energy range.

## 2. Inelastic Scattering

Differential cross sections for inelastic scattering of protons from two excited levels of carbon have been measured at a sufficient number of angles to make a good comparison to the theory of inelastic scattering proposed by Austern, Butler, and McManus.<sup>12</sup> In this theory the angular dependence is

$$\frac{d\sigma}{d\omega} \sim \left[ j_{\ell}(ga) \right]^2 ,$$

where  $a$  is a measure of the radius of the peripheral region in which the scattering takes place and  $\ell$  is the change in angular momentum of the incident and scattered protons. This change  $\ell$  is related to the change in angular momentum  $\Delta J$  between initial and final nuclei by  $\Delta J = \ell \pm 1$  or  $0$  (i. e., contribution due to proton spin is  $\pm 1$  or  $0$ ). However, the position of the first observed maximum in the angular distribution determines the minimum value of  $\ell$  where

$$\ell_{\min} = \left| \vec{J} + \vec{J}' + \vec{1} \right|_{\min} .$$



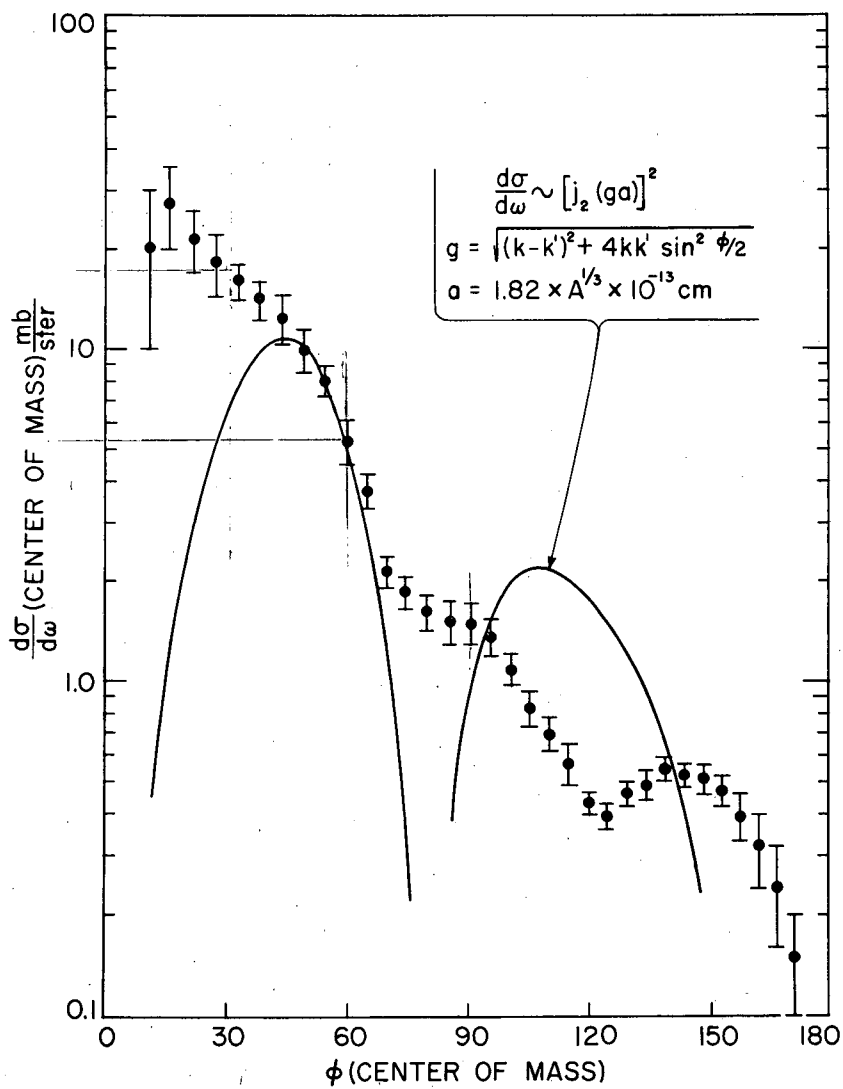
The parity of the wave function representing the excited state is the same as ( $\ell$  even) or different from ( $\ell$  odd) that of the ground state. For  $C^{12}$ ,  $J = 0^+$  for the ground state.<sup>14</sup> Thus a peak in the angular distribution directly forward ( $\ell_{\min} = 0$ ) would indicate that  $\Delta J$  ( $= |J - J'|$ ) is 0 or 1 with no change in parity. If there is no peak directly forward ( $\ell_{\min} > 0$ ) then either  $\Delta J \geq 0$  with a change in parity or  $\Delta J \geq 2$  with no parity change. The general rule then is:

if  $\ell_{\min} = 1$ , then  $\Delta J = 0, 1$ , or  $2$ ;

if  $\ell_{\min} \neq 1$ , then  $\Delta J = \ell_{\min}$ , or  $\ell_{\min} + 1$ .

The cross sections of the first excited level of  $C^{12}$  are well defined at all angles and produce the angular distribution shown in Fig. 10. Probable errors are as high as 50 percent for  $10^\circ$  and  $170^\circ$ , but for most points are between 10 and 20 percent and include all sources of error in the absolute value of the differential cross section. Relative cross sections are more reliable by a factor of at least two.  $J = 2$  for this level,<sup>14</sup> so allowable values of  $\ell$  are 1, 2, and 3. However, the parity is also known to be even, consequently the odd values of  $\ell$  are eliminated and there results the unequivocal choice for  $\ell$  of two units. Thus, for this level, instead of predicting a  $\Delta J$  and hence  $J'$ , it is only necessary to see if the observed distribution matches that of  $j_2(\text{ga})$ .

A plot of  $j_2$  for  $a = 1.82 \times A^{1/3} \times 10^{-13}$  cm is shown in Fig. 10. This choice of nuclear radius is equivalent to requiring the maximum of the first lobe of the Bessel function to fall at  $40^\circ$ . If the argument of  $j_2$  is adjusted so that the maximum falls at  $15^\circ$ , to correspond to the observed data, the value obtained for the nuclear radius is  $4.5 \times A^{1/3} \times 10^{-13}$  cm, which has little meaning. Furthermore, the shape of the first lobe becomes far too narrow and many lobes appear over the angular range which bear no relation to the observed distribution. Going to values of  $a$  less than  $1.8 \times A^{1/3} \times 10^{-13}$  cm produces a maximum where none appears in the data and results in essentially only one lobe extending over most of the angular range. It might seem that the plotted distribution could be considered a fit if there were evidence of some other process (e.g., slit scattering) contributing to the higher cross sections at angles less than  $40^\circ$ , but no such process



MU-9312

Fig. 10. Angular distribution of the differential cross section for the reaction  $p + C^{12} \rightarrow p' + C^{12*}$  (4.43 Mev) and the Austern, Butler, and McManus prediction

was found. The data are also verified by results from the differential range spectra for this level. The conclusion is drawn that this simple theory is inadequate.

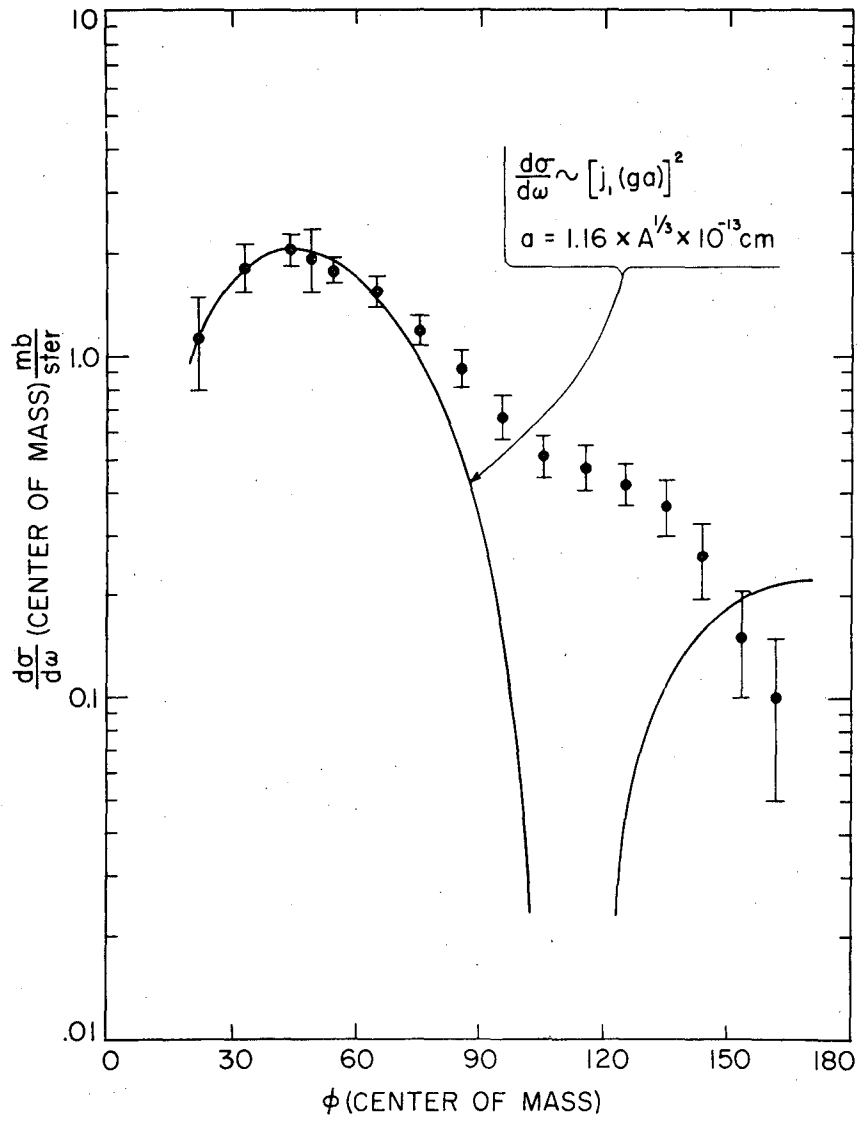
The angular distribution of protons corresponding to the third level ( $\epsilon = 9.6$  Mev) is shown in Fig. 11. Data were taken every  $10^\circ$  from  $20^\circ$  to  $160^\circ$  (lab) with the differential range spectrometer. The spin and parity of this level are not known.

The general shape of the angular distribution at forward angles is given by  $j_1$ . Distributions for  $j_0$  are peaked at  $0^\circ$ , while  $j_2$  and higher produce distributions which, when normalized to peak at the experimentally observed value of  $\theta = 40^\circ$ , are too narrow to fit the data. The best fit is given by  $j_1$  with  $a = 1.16 \times A^{1/3} \times 10^{-13}$  cm. Poorer fits to the observed distribution could be made for  $a = 1.20 \times A^{1/3} \times 10^{-13}$  cm as well as  $1.10 \times A^{1/3} \times 10^{-13}$  cm. The fit to the data shown in Fig. 11 is about as good as any obtained for beryllium. The value obtained for the nuclear radius perhaps should not receive any great weight, but should be within reasonable limits, i. e., between 1.0 and  $2.0 \times A^{1/3}$  cm. That a fit can be made to the data at forward angles is significant in this theory, since this defines  $\ell_{\min}$  and thus introduces information about  $\Delta J$ . In this case then  $J' = 0, 1$  or  $2$  with a parity change.

The deviation from  $j_2$  of the observed experimental angular distribution for the first excited level at forward angles may in part be due to the use of the impulse approximation in the theory. The wave function representing the incident proton is considered to be undisturbed by the presence of the nuclear potential. In their paper, Austern, Butler, and McManus show that a correction for the effect of the nuclear potential raises the height of the predicted distribution at small angles and shifts the first maximum somewhat forward, both of which effects seem to hold for this level. There would be real value in determining the spin and parity of the third level independently to see if the fit with  $j_1$  is merely fortuitous.

### 3. Deuterons

The angular distribution of the pickup deuterons from the  $C^{12}$  (p, d) $C^{11}$  reaction has been compared with the prediction of Butler



MU-9311

Fig. 11. Angular distribution of the differential cross section for the reaction  $p + C^{12} \rightarrow p' + C^{12*}$  (9.60 Mev) and the Austern, Butler, and McManus curve for  $\ell = 1$

stripping theory, which gives

$$\frac{d\sigma}{d\omega} \sim f(K) \left[ A_{\ell} j_{\ell}(Zr) + \left( \frac{Zr}{2\ell+1} \right) B_{\ell} \left\{ \ell j_{\ell-1}(ZR) - (\ell+1) j_{\ell+1}(Zr) \right\} \right]^2$$

where

$$f(K) \sim \left\{ \frac{1}{K^2 + a^2} - \frac{1}{K^2 + (a+b)^2} \right\}^2 \quad (\text{Fourier transform of deuteron wave function})$$

$$\text{and } K = \sqrt{\left( \frac{1}{2} k_d - k_p \right)^2 + 2k_d k_p \sin^2 \phi / 2},$$

$$a = 2.32 \times 10^{12} \text{ cm}^{-1}, \quad b \simeq 6a,$$

$$Z = \sqrt{(k_d - k_p)^2 + (4k_d k_p \sin^2 \phi / 2)},$$

$$r = \text{sum of the radii of deuteron and nucleus} \\ \simeq 1.4(A^{1/3} + 1) \times 10^{-13} \text{ cm},$$

$$A_{\ell} = \sum_{n=0}^{\ell} \frac{(\ell+n)! (k_s r + n + 1)}{n! (\ell-n)! (2k_s r)^n}, \quad B_{\ell} = \sum_{n=0}^{\ell} \frac{(\ell+n)!}{n! (\ell-n)! (2k_s r)^n},$$

$$k_s = -ik_n, \quad k = \frac{\sqrt{2ME}}{\hbar}.$$

If the shell-model prediction<sup>25</sup> of  $J = \frac{3}{2}^-$  for the ground state of  $C^{11}$  is assumed, possible values of  $\ell$  (the angular momentum carried by the picked up neutron) are 1 and 3.

Figure 12 is a comparison of a Butler-prediction curve for  $\ell = 1$  and a curve drawn through the experimental points. Although more data points would be desirable, the character of the sharp rise at forward angles is definite and the similarity in shape at larger angles suggests a reasonable fit. Efforts to match Butler predictions for  $\ell = 0, 2,$  or  $3$  were unsuccessful. Thus, the results are consistent with the assumption that the ground state of  $C^{11}$  is  $\frac{3}{2}^-$  with odd parity.

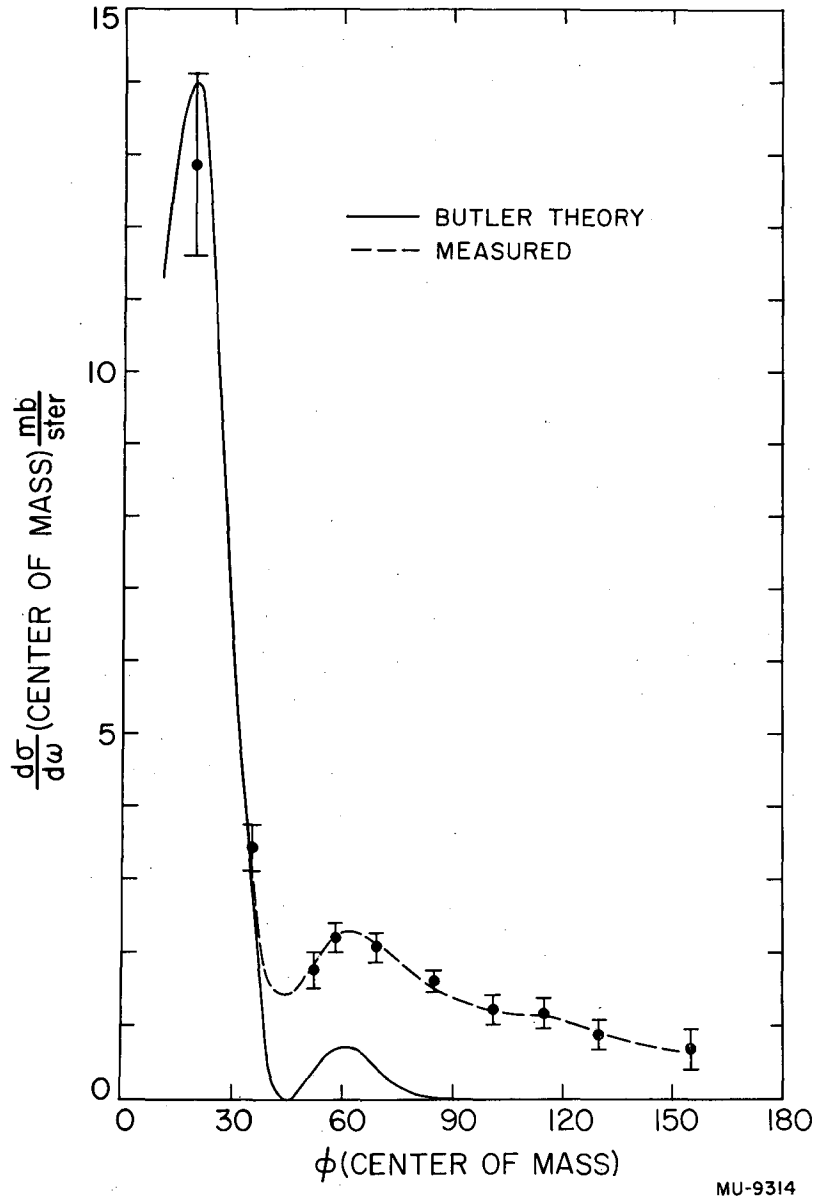


Fig. 12. Angular distribution of the differential cross section for the production of deuterons by the reaction  $p + C^{12} \rightarrow d + C^{11}$  and the Butler Theory prediction

MU-9314

ACKNOWLEDGMENTS

The author is indebted to

Professor Luis W. Alvarez for his interest and encouragement,  
Dr. Reinald G. Finke and Mr. Robert Silver for their active  
participation in all phases of the work,

Dr. Jack Benveniste for the use of some carbon spectra taken  
earlier,

Dr. Warren Heckrotte for several illuminating discussions on  
inelastic scattering and Butler stripping theory,

Mr. William Gantz of the Electronics Group for his capable  
maintenance of the electronic equipment,

And, finally, all members of the linear accelerator crew.

This work was done under the auspices of the U. S. Atomic  
Energy Commission.

REFERENCES

1. V. F. Weisskopf, *Helv. Phys. Acta.* 23, 187 (1950)
2. J. M. Blatt and V. F. Weisskopf, "Theoretical Nuclear Physics," Wiley (1952)
3. L. Wolfenstein, *Phys. Rev.* 82, 690 (1951)
4. J. M. Blatt and V. F. Weisskopf, Technical Report No. 42, M.I.T. (1950)
5. S. Fernbach, R. Serber, and T. B. Taylor, *Phys. Rev.* 75, 1352 (1949)
6. E. H. Roderick, *Proc. Roy. Soc. (London)* 201, 348 (1950)
7. H. E. Gove and H. F. Stoddart, *Phys. Rev.* 86, 572 (1952)
8. C. J. Baker, J. N. Dodd, and D. H. Simmons, *Phys. Rev.* 85, 1051 (1952)
9. G. E. Fischer, *Phys. Rev.* 96, 704 (1954)
10. R. Britten, *Phys. Rev.* 88, 283 (1952)
11. R. M. Eisberg and G. Igo, *Phys. Rev.* 93, 1039 (1954)
12. N. Austern, S. T. Butler, & H. McManus, *Phys. Rev.* 92, 350 (1953)
13. R. G. Finke, University of California Radiation Laboratory Report No. UCRL-2789 (1954)
14. F. Ajzenberg and T. Lauritsen, *Rev. Mod. Phys.* 27, 77 (1955)
15. R. E. LeLevier and D. S. Saxon, *Phys. Rev.* 87, 40 (1952)
16. B. L. Cohen and R. V. Neidigh, *Phys. Rev.* 93, 282 (1954)
17. S. T. Butler, *Proc. Roy. Soc. (London)* A208, 559 (1951)
18. P. B. Daitch and J. B. French, *Phys. Rev.* 87, 900 (1952)
19. L. W. Alvarez et al., University of California Radiation Laboratory Report No. UCRL-236 Rev. (1953)
20. H. R. Bowman and R. E. Thomas, University of California Radiation Laboratory Report No. UCRL-2164 (1954)
21. J. Benveniste, University of California Radiation Laboratory Report No. UCRL-1689 (1952)
22. J. Benveniste and B. Cork, *Phys. Rev.* 89, 422 (1953)
23. V. J. Ashby, University of California Radiation Laboratory Report No. UCRL-2091 (1953)
24. J. H. Smith, *Phys. Rev.* 71, 32 (1947)
25. M. G. Mayer, *Phys. Rev.* 78, 16 (1950)